Chapter 1

Exploring the linearity of the climate response to external forcing

1.1 Introduction

In recent decades, increasing concern has been voiced about the impact of man made emissions into the atmosphere. Attention has moved from considering the local effects of polluting gases to the affect that green house gases might play on the global climate. Evidence that the so called green house gases (ghg) might one day be responsible for large scale temperature change began to gain credence in the late 60's early 70's. As the science behind the role that ghgs might play on the global atmosphere became clearer the debate shifted to consider whether observed changes in the climate could be identified. The record of sea surface temperature and land based climate measurements indicated a warming in global temperature in the early part of the century. However it remained a point of contention in the research community whether the observed changes could be accounted for by natural changes (in the sun's activity or volcanic emissions) and internal variability of the climate system or whether the changes could be attributed to the impact of anthropogenic emissions. As our ability to use numerical tools to model the global climate improved and as the stronger warming signal from the nineteen eighties onwards appeared, the question of whether human induced climate change is occurring has largely been resolved.

State of the art computer models are used in the simulation of the global climate (based on fundamental equations governing fluid-dynamical flow) are able to reproduce many of the observed characteristics

of the atmosphere and ocean. The process of modelling the earth's climate uses vast computational resources and involves modelling transport and radiative processes over a 3D discretised grid. A typical modern Atmosphere Ocean Global Circulation Model (AOGCM) resolves the interactions between the various climate components: the atmosphere, the ocean, the cryosphere (ice sheets) and the land surface and biosphere. In these models, changes in anthropogenic emissions and the strength of the solar activity are treated as external forcings on the radiative balance of the global climate. The model resolves the response of the various feedback process in the climate to any changes. The fact that these AOGCMs, based on the so called primitive equations can reproduce recent climate change gives confidence that the model climates are responding in a realistic manner to the imposed radiative forcings. Since the first Inter-governmental Panel on Climate Change (IPCC) report was commissioned in 1991 these models have increasingly been used to produce future climate forecasts based on projected scenarios of future anthropogenic emissions of ghgs and other gases.

The models which have been used in subsequent IPCC reports have been developed by a range of research groups in Europe, the Americans, Japan and Australia. The different ways each of these models represent specific processes in the climate (e.g. cloud formation, ocean heat exchange or land surface albedo changes for instance) has meant that the range of models produce a range of future climate predictions for an identical future emission scenario. As the models each manage to reproduce the main features of recent climate, this spread of future forecasts is an indicator of a range of climate responses. Cubasch et al. (2001) and Kattenberg et al. (1996) give the range of global temperature change in 2050 and 2100 for a set of given future ghg emission scenarios based on the range of model responses available. The usefulness of this predicted range is limited as an assessment of uncertainty as no weight on the likelihood of a given model projection can be extracted. A more systematic approach to assessing uncertainty in future forecasts has been taken by Allen et al. (2000) and Stott and Kettleborough (2001), who produce probability density functions (pdfs) for future global temperature change by combining pdfs due to individual uncertainties in the climate.

Earth's climate exhibits a whole range of responses to changes in the radiative forcing imposed on the atmosphere. If we consider the case of an increase in the radiative forcing at the top of the atmosphere (by this we mean the change in the net heat flux into the atmosphere as a result of increases in ghg concentrations or an increase in solar activity) then the atmosphere can respond in a variety of ways. For example, producing large scale albedo changes (as the result of snow cover changes or increased cloud cover) or increased atmospheric water vapour (which itself is a ghg) as a result of a warmer troposphere. The strengths and the way that these competing feedbacks combine in the real climate is difficult to assess and the uncertainty which exists is evident in the way climate models seek to parameterise these

processes. The overall sensitivity of the climate to a given change is dependent on the magnitude of the combined feedback processes. The degree to which a climate model over- or under-predicts these feedback processes will determine the degree to which the equilibrium response to any changes will be over- or under-predicted.

Ocean processes and Atmosphere-Ocean interactions also require consideration. Of particular importance is the efficiency of the penetration of heat into the deeper ocean. The ocean, which has a much greater heat capacity than the atmosphere, controls the rate that the climate comes into equilibrium with any changes. Understanding the processes by which heat penetrates into the deeper ocean is vital for assessing the time scale of climatic response. Due to the sparse nature of our current oceanic data, the role of the ocean in uptake of heat is poorly understood.

Current models provide some indication of the range of uncertainty in the efficiency of ocean heat uptake. The full AOGCMs have no explicit parameterisation of the climate sensitivity or heat uptake by the ocean, though these properties are diagnosable from the response of the model using simple models. Simpler models (such as energy balance models) can be tuned to reproduce the response of AOGCMs and the parameterisation of climate sensitivity and heat uptake in these models can be used to establish the properties of the more complex AOGCMs. Analysis of the current AOGCMs suggests a wide range of diffusion parameters (Sokolov and Stone (1998), Sokolov and Stone (1996)) from near 0 to 50 $cm^2 s^{-1}$. The range of uncertainty in this parameter can not be expected to be fully explored by the current range of AOGCMs and is likely to be larger.

Forest et al. (2000) and Forest et al. (2002) use optimal fingerprint techniques, developed in the attribution and detection literature, to place constraints on the key climate parameters which are consistent with recent climate change. These studies are sufficient to place a lower bound on the climate sensitivity (for all parameterisation of ocean heat uptake). Forest et al. (2002), by including additional information on the change in the heat content in the ocean from Levitus et al. (2000), provide an upper limit for climate sensitivity. No useful limit could be placed on the ocean heat uptake in these studies.

It is the combination of the uncertainty in the feedback mechanisms in the climate and hence the sensitivity of the climate to any radiative change and the role that the ocean plays in surface heat uptake that makes it difficult to constrain estimates of these uncertainties by use of the recent climate record. However reproduction of recent climate change is used as a constraint on errors in short time scale (decadal to century) climate forecasts. Current forecasts use the assumption that errors in the reproduction of past changes due to climate sensitivity and ocean heat uptake uncertainties will be persistent for future predictions. On this basis we assume that a model which over or under predicts

recent observed climate change will continue to over- or under-predict climate change by a similar amount in the future. Climate model responses reconciled with recent climate can be expected to produce a realistic short term future climate response. Analysis using a simple model (Allen et al. (2000)) suggests that such errors associated with this assumption are minimal over a 100 year forecast period based on the evaluation of the persistence of errors for a portion of the parameter space. This finding is useful for uncertainties in a region of parameter space which was assess for that specific future emission scenario but needs to be extended to the full range of uncertainty in the key parameters and to cover other future emission scenarios. The future ghg emission scenario used was a scenario produced for the Second Assessment Report, Kattenberg et al. (1996). This report aims to make a systematic assessment of the impact of this assumption for the whole of the parameter space of climate sensitivity and ocean diffusivity consistent with the recent record. This will be done to assess errors in the scaling for four of the current future emission scenarios used in the Third Assessment Report, Nakicenovic et al. (2000).

1.2 Examining key climate parameters using a simple model

To explore the impact of uncertainty in the key climate parameters, climate sensitivity and heat uptake by the deep ocean, this study uses a simple energy balance model (EBM). These models see a wide range of applications in the climate research community, where they have been used to explore the equilibrium response to atmospheric changes (e.g. Hansen et al. (1980)). These models are also used widely for extending the range of forecasts for future scenarios, Cubasch et al. (2001). The model predicts the global temperature response to changes in radiative forcing (induced by changes in the atmospheric composition or solar activity), and as such deals with the globe as a 0D/1D model.

In simple thermodynamic terms we can express the change in temperature with time in terms of the imposed radiative flux due to an applied forcing (Q) on the climate system and the radiative response of the system to that forcing.

$$C_{\mathrm{ml}}\frac{d\Delta T}{dt} = Q - \lambda\Delta T \tag{1.1}$$

where C_{ml} is the heat capacity of the mixed layer, ΔT is the surface temperature response and λ is the climate feedback parameter. The climate feedback parameter (λ) represents the linearisation of the combined feedback processes in the climate for the range of possible radiative forcings. This linearisation appears to be justified on the basis of feedback responses observed in full AOGCMs. λ is a measure of

the strength of the combined feedback mechanisms to radiative changes. The model is used to simulate a change in surface temperature from it's initial state due to changes in radiative forcing. The upper portion of the ocean is marked by rapid mixing which ensures that this homogeneous region responds on relatively short time scales to atmospheric changes. Strong stratification below the mixed layer separates the warmer surface waters from the colder deep waters in a region known as the thermocline. The mixed layer contains the bulk of the heat capacity in the rapidly responding region of the climate (the atmosphere and upper ocean). The response of the ocean mixed layer is used in this model, to evaluate the surface climate response. In the later work in this report this zero dimensional model is extended to include parameterisation of heat exchange with the deeper ocean below this mixed layer, but for this initial exploration of the model the assumption is made that negligible heat exchange occurs across the thermocline.

From equation 1.1 we can see that the equilibrium temperature response of such a model to a step change in forcing Q_0 (instantaneous increase), where the $\frac{d\Delta T}{dt}$ term approaches zero, is given by:

$$\Delta T_{\mathrm{eq}} = \frac{Q_0}{\lambda} \tag{1.2}$$

The equilibrium temperature response of the model is referred to as the climate sensitivity to the given change in forcing (in an analogous way to that used in GCM analysis, Senior and Mitchell (2000)). For inter-model comparison purposes we more commonly use the equilibrium temperature response ($\Delta T_{eq2*CO2}$) to the radiative forcing imposed due to doubling of atmospheric CO_2 levels when referring to the climate sensitivity.

$$\Delta T_{\mathrm{eq2*CO2}} = \frac{Q_{2*\mathrm{CO2}}}{\lambda} \tag{1.3}$$

The values for sensitivity given in this study are given on this basis. λ (which relates the radiative forcing associated with the doubling of CO_2 ($3.74\,W\,m^{-2}$ in HadCM3) to the equilibrium temperature response ($\Delta T_{eq2*CO2}$)) is not specific to the forcing scenario. The radiative forcing (Q_0) is defined for the more complex stratosphere resolving AOGCMs, as the radiative flux imposed at the top of the atmosphere. However as the stratosphere adjusts quickly to radiative changes it is common to use the radiative flux at the tropopause as the measure of radiative forcing.

Equation 1.1 can be solved for the temperature response of the Energy Balance Model (EBM) as shown below for an instantaneous step increase in forcing (Q_0 (in the general case Q is a time dependent

property)):

$$\Delta T = \frac{Q_0}{\lambda} - \frac{Q_0}{\lambda} exp \frac{-\lambda t}{C_{\mathrm{ml}}} \tag{1.4}$$

The $e-$folding time scale of the temperature response of this model is defined by C_{ml}/λ. The time scale is dependant on the heat capacity of the mixed layer and the strength of the climate feedbacks, as defined by the climate sensitivity parameter (λ - equation 1.3). The climate feedback parameter is inversely related to the equilibrium climate temperature response, or climate sensitivity, so we can say that a climate system with a large heat capacity or a large climate sensitivity would have a longer response time to any changes. In simple terms a model representing a climate with weak climate feedbacks to applied forcing would be expected to respond quickly because feedback processes will scale with the temperature not the forcing.

The time scale of response of the ocean mixed layer can be estimated. Assuming a 100m depth for an ocean which covers 70% of the globe and a climate feedback parameter calculated from the parameterisation of sensitivity in the Hadley Centre GCM (HadCM3, $\Delta T_{eq2*CO2} = 2.7$) and the top of the atmosphere flux for the doubling of CO_2 ($Q_{2*\mathrm{CO2}} = 3.74\ Wm^{-2}$), the $e-$folding response time for this model can be shown to be of the order of 6.3 years for a doubling in CO_2.

If we consider the first 2 terms of the Taylor expansion of the exponential term in equation 1.4 we can say that for small time scales (t) that the temperature response of the model is approximately independent of λ (and hence the climate sensitivity).

$$\Delta T = \frac{Q_0 t}{C_{\mathrm{ml}}} \tag{1.5}$$

Therefore, at the point where a step change in forcing is applied, the gradient of the temperature response will be defined by the forcing and heat capacity of the model only. Consequently, on short time scales the response of the model to a step change in forcing is not dependant on the parameterisation of the climate sensitivity.

We can consider the case where the model is forced by a time dependent radiative forcing profile (Q) which is defined as a forcing rate α. We can derive an equation similar to equation 1.4 using integration factors as given below:

$$\Delta T = \frac{\alpha t}{\lambda} - \frac{\alpha C}{\lambda^2}(exp \frac{-\lambda t}{C_{\mathrm{ml}}} - 1) \tag{1.6}$$

The temperature response at any given time is dominated by the response of the recent increase in forcing (α) while the differences in the longer term response to less recent forcing (for differing climate

sensitivity values) has less impact. When the model is forced by an non-uniform increase in Q these differences in the stabilisation of the model parameterised with different climate sensitivities become apparent. The degree that future forcing scenarios diverge or remain close to a continuously increasing profile forms the basis of the scaling assumption and is explored in more depth later in this chapter.

So far we have considered the temperature response of the shallow well mixed surface layer. Although this represents the majority of the heat capacity if just the atmosphere and mixed layer is considered, the mixed layer only accounts for only a small proportion of the total heat capacity of the ocean. If we where to consider the response of the whole ocean (assume that the ocean mixed layer was 4000 m in depth for instance) we can show that the response time scale of such model is of the order 250 years. This however would be an underestimate of the true oceanic response time due to the restriction of heat transfer between the surface layers and the deeper ocean waters by strong stratification at the thermocline. It is known that transfer of heat, salinity and other ocean properties occur across this boundary, but this is a spatially non-uniform process, and is complicated by strong localised overturning in parts of the ocean, as well as the interaction of salinity gradients in addition to the thermal gradients. This remains one of the key unknown properties of the climate system. The rate that heat is absorbed by the deeper ocean is important because it controls the time scale with which the surface temperature comes into equilibrium with any radiative changes.

For the purposes of the energy balance model we can introduce an additional term to parameterise this heat exchange between the oceanic mixed layer and the deeper ocean. Equation 1.1 becomes:

$$C_{\mathrm{ml}}\frac{d\Delta T}{dt} = Q - \lambda\Delta T - \rho C_{\mathrm{w}} K_{\mathrm{v}} \frac{dT}{dz})_{\mathrm{z}=0} \tag{1.7}$$

where K_{v} is a ocean diffusivity parameter and $\frac{dT}{dz})_{\mathrm{z}=0}$ is the temperature gradient at the base of the mixed layer. The T parameter defines the depth dependent temperature which differs from ΔT (which is the global surface temperature change from the climate equilibrium state) The strength of the heat uptake into the deeper ocean is controlled by the strength of the diffusivity term, K_{v}. Heat transfer in the interior of the ocean is governed by the diffusion expression:

$$\frac{d^2T}{dz^2} = \frac{1}{K_{\mathrm{v}}}\frac{dT}{dt} \tag{1.8}$$

It is now possible to solve the surface temperature response numerically by resolving the depth and time dependent temperature response. A similar response can be calculated in a computationally less intensive manner by assuming that the heat flow is into an ocean of semi-infinite depth. Following

Holman (1986), we can show that the heat flux at the base of the ocean mixed layer can be given by:

$$C_{\mathrm{ml}}\frac{d\Delta T}{dt} = Q - \lambda\Delta T - \rho C_{\mathrm{w}}\sqrt{\frac{K_{\mathrm{v}}}{\pi}}\int \frac{1}{\sqrt{t}}\frac{d\Delta T}{dt}dt \tag{1.9}$$

This expression, which governs the surface temperature response is used as the prognostic equation for the work detailed in this report. A 1 dimentional model was also coded to resolve the time and depth dependent response (as defined by equations 1.7 and 1.8) so that the results can be compared with the formulation using equation 1.9, which showed comparable results over the 200 year timescales that we consider here.

In practise a large portion of the heat exchange occurs by non-diffusive processes but as most heat transport occurs down gradient a simple diffusion parameterisation is a sensible 1st order approximation for the purposes of determining the global temperature response. Increasing surface heating can be expected to increase the stratification at the thermocline, stabilising the water column. Parameterising the heat transfer as a global diffusive property, enables us to explore the effect of varying the strength of this heat exchange.

While it may be possible to derive an analytical solution (analogous to equation 1.4) from equation 1.7, the effect of the additional heat transfer into the deeper ocean can be qualitatively inferred from the behaviour of the simpler system described for the mixed layer response. Increasing the heat flux into the deeper ocean, can be seen as increasing the available heat capacity of the system as a whole, allowing us to introduce the concept of an effective heat capacity. In a similar way that increasing the climate sensitivity and the heat capacity of the mixed layer increases the response times of the model, so parameterising a larger ocean diffusivity (K_v) will result in a larger effective heat capacity which will also increase the model response time.

Scale-ability of predictions The energy balance model (EBM) gives us the flexibility to systematically study the effect of varying climate sensitivity and the rate of deep ocean heat uptake. To illustrate the stabilisation response for a range of model parameterisations in the EBM, 900 model simulations where carried out for each point on a 2D parameter space consisting of climate sensitivity (varying between 0.5 to 15 K) and ocean diffusivity (varying between 0.03 and 50 cm^2s^{-1}) over a regular 30 by 30 grid. This parameter space was selected to explore the range of parameters which Forest et al. (2000) could not rule out as being inconstant with recent climate change. The model was forced with a instantaneous increase in radiative forcing in 1900 and then allowed to come into equilibrium through the next 200 years. No further forcing was introduced through this period The stabilisation response

such as that produced by introducing a step change can be explored for varying combinations of parameterisations. The pattern of response is useful in suggesting the region of parameter space where the behaviour of the temperature response in the model is likely to differ from a given reference response. A AOGCM forecast can be seen as a reference response. We can use the EBM to explore the ability of a given model parameterisation to capture the temperature response of a 'true' parameterisation which can be expected to be found in the parameter space.

At this stage it is important to introduce the concept of 'scale-ability'. In the process of making climate forecasts, an assessment of uncertainty is vital if value is to be placed on the predictions regardless of the tools used (be they Intermediate complex-ability models or the full AOGCMs). Given that we are not able to place constraints on the uncertainties of the two key climate parameters (climate sensitivity and heat uptake by the deep ocean) we instead need to use the recent climate change as a constraint on future forecasts. The scaling assumption is based on the principle that the errors involved in the reproduction of recent climate trends will be consistent with errors associated with future predictions. Uncertainties in the climate parameters will lead to break down of this relationship on longer timescales but Allen et al. (2000) demonstrates that for selective regions of parameter space that this assumption holds for century scale predictions. The scaling relationship is the assumption that errors in the reproduction of past changes will scale with errors in future temperature projections.

The ranges of possible values for these two parameterisations can only be poorly constrained by the observed record to date (Forest et al. (2000) and Forest et al. (2002)). This uncertainty means that predicting the temperature response to a stabilisation in forcing using a climate model (which is able to reproduce the past climate record but uses values for these two parameters which differ markedly from the real climate system) could produce a very different temperature response to that of the actual climate response.

The small skill level inherent in estimation of stabilisation climates (climates which approach equilibrium with any introduced radiative changes) does not as might be expected, limit completely the model skill at making short term climate forecasts (decadal to century time scale). As noted briefly earlier, the stabilisation response of the differing parameterisations isn't relevant for scenarios of radiative forcing profiles which have a steady increase over time. In this case the later temperature response would scale with the earlier temperature similarly across the parameter space.

If we define this as the scale-ability relationship then we can assume that if errors in parameterisation of climate models cancel in the reproduction of the observed climate record then the errors can be expected to continue to do so for the duration of the period where scale-ability holds true. In this

way the reproduction of past climate change is a good constraint on errors in future forecasts as long as the scale-ability assumption holds (i.e. for as long as models are driven by continually increasing radiative forcing). Scale-ability is a less restrictive concept than considering the linearity of response. The response can be non-linear with respect to key parameters but still scale-able over a given timescale.

1.3 Stabilisation response

The stabilisation response of the model represents an extreme forcing scenario which illustrates the potential for a breakdown in scale-ability. The temperature realisation of the model to step change in radiative forcing illustrates the varying time scales of response. Figure 1.1 shows the temperature realisations for 8 parameter combinations taken from these 900 runs. These 8 show the range of response behaviours found in the stabilisation scenario. While all the parameterisations lie within the region consistent with the recent climate record (Forest et al. (2000)) the individual responses to stabilisation in forcing show very different outcomes. This range of responses in the 8 realisations chosen for figure 1, illustrate the difficulty in making longer term (or equilibrium) climate prediction. Climate models using one set of parameters to represent the climate would show very little skill in reproducing a real climate with parameter values of one of the other 7 combinations.

Three of the realisations correspond to parameterisations with near zero ocean diffusivity ($0.03\ cm^2 s^{-1}$) but with a range of climate sensitivities (long dash (ΔT_{eq}=12), dark blue (ΔT_{eq}=6) and dash-dot (ΔT_{eq}=0.5)). The behaviour of these realisation closely matches the behaviour predicted by the mixed layer only response of the EBM and we can see many of the features of this model in these responses. The eventual climate for all three realisations is very different (equal to Q/λ where $\lambda = Q_{2co2}/\Delta T_{eq2co2}$) but the early temperature response in each case is similar to the others (being independent of λ), 1.6.

The shape of the model responses and their scale-ability over the 200 years can be explained in terms of the response time scales of the models. Model runs using larger values for climate sensitivity and ocean diffusivity (K_v) and hence longer time scales, show responses which are close to scaled versions of each other through the runs. The central parameter combination (black line, ΔT_{eq}=6, K_v=12), the largest parameter combination (short dash, ΔT_{eq}=12, K_v=25) and a model run parameterised with modest values (green, ΔT_{eq}=3.5, K_v=4.75) all fall into this category. The response time scales for all these runs is larger than the time scale observed in this step change simulation (200 years) and as such the differences between model parameter combinations isn't evident at this stage. The assumption of a scaling relationship holds well for models parameterised in this region of parameter space even in

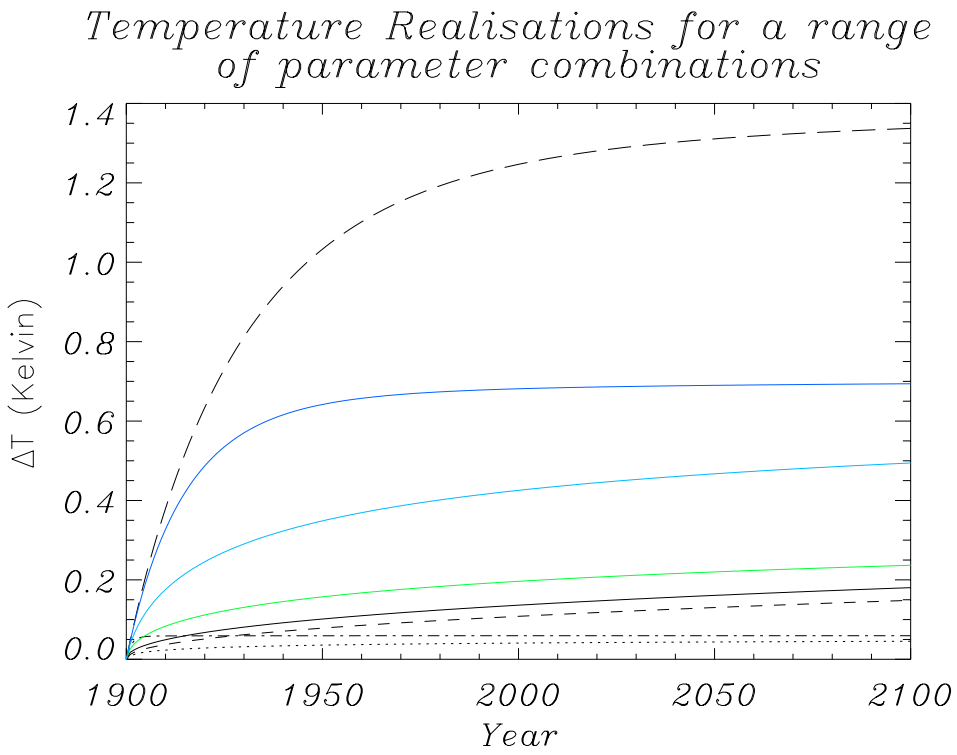

Figure 1.1: .The temperature realisation for 8 parameter combination in response to a step change in forcing. The black solid line represents a combination central to the parameter space (ΔT_{eq}=6 and K_v=12). The four dashed lines represent parameter combinations from the 4 corners of parameter space, long dash (ΔT_{eq}=12, K_v=0.03), short dash (ΔT_{eq}=12, K_v=25), dash-dot (ΔT_{eq}=0.5, K_v=0.03) and the dotted line (ΔT_{eq}=0.5, K_v=25). The impact of small ocean diffusivities is illustrated by the temperature response of the two high sensitivity cases (two dashed lines). The timescale of response of the long dashed case is sufficiently short that temperature stabilisation of the model is evident on the 200 year timescale. The short-dashed combination, while sharing the same eventual temperature response, only realises a small fraction of this temperature response to the step change in this time period Similarly the response of the two low sensitivity cases (dot-dashed and dot-dot) show a similar picture. The shorter timescales for response inherent in the small sensitivity, small K_v(dot-dot) result in the vast majority of the response being realised in the first couple of years (Note. The early response (first couple of years) is similar to the response of other combinations (long dashed and dark blue) which share the equally low ocean diffusivity). The small sensitivity, large K_v(dot-dashed), while sharing the same temperature response has only realised 80% of this after the first 200 years. The 3 coloured lines represent intermediate responses. The Dark blue line (ΔT_{eq}=6, K_v=0.03) illustrates that though the later response temperature response is half that of the final long-dashed line the early temperature response is very similar for both combinations. The lighter Blue line (ΔT_{eq}=6, K_v=0.59) represents a response with a small increase in the ocean diffusivity to that of the dark line. The early responses of the the two blue lines are not scaled responses of each other, though the eventual temperature realisation will be the same. The Green line (ΔT_{eq}=3.5, K_v=4.75) corresponds to a modest estimate of sensitivity and ocean diffusivity. The response does not scale well with the combinations with low sensitivity or ocean diffusivity, but shares more in common with the response of the parameter combinations in the remainder of the parameter space (solid and small-dashed lines).

stabilisation scenarios and errors between models in this region would not be evident on these time scales. The bulk of parameter space falls into this category, with only models with small parameter values (for either climate sensitivity or the ocean diffusivity) showing a diverging response behaviour.

The three model runs with small ocean diffusivities (mentioned above) fall into this category as well as the small sensitivity and large ocean diffusivity case (dot-dot). Responses of the models with parameterisations in the small sensitivity or small ocean diffusivity region are not homogeneous, showing large differences in scale-ability the same region. The light blue line is produced with a model with identical sensitivity to the dark blue response but with marginally larger ocean diffusivity (K_v=0.59 as compared with 0.03 cm^2s^{-1}). The responses of these two do not scale well over this period, while at the same time the responses of the bulk of the model parameter space is different again. Errors based on making a scaling assumption can be expected if either the climate model used for prediction or the real climate's parameters lie within this region. Idealised experiments using stabilisation to step changes in forcing are useful in being able to predict regions of parameter space where errors can be expected.

Figure 2 illustrates the same behaviour by looking at the ratio of the warming between 2000-2050 to the warming between 1900 and 2000 for the same step change (in 1900) experiments. The plot shows ratio contours for the complete parameter space involved in the discussion above. The magnitude of the ratios on the plot is not important. If the reference model parameterisation and the true values of the climate both lie in the same contour then the scaling assumption holds. If however the reference and the true values are separated by contour lines then errors are introduced into the ability of the reference model to scale with the true climate response. The magnitude of these errors introduced by this break down in scale-ability is dependent on the number of contours which separates the reference and the true values. As already noted, the bulk of the parameter space (green contours) over century time scales remains close to a scale-able response. The region with smaller values for the two key parameters show marked break down in the scaling ratio (as indicated by the large number of contours). For stabilisation scenarios, differences between temperatures predicted by a climate model and the temperature response of the real climate will depend on the number of contours between their respective parameter values. As this range of parameters involved in this plot can not be ruled out as inconsistent with the observed climate history, consideration of the errors due to the breakdown in scale-ability needs to be considered in any assessment of the uncertainty in climate predictions.

1.4 Assessment of error due to the scaling assumption for SRES scenarios

In the earlier sections we examined the use of a simple energy balance model (EBM) to explore the potential for the introduction of error due to the break down in scale-ability of future temperature change by looking at an idealised response to a step change in forcing. We are also able to make a more quantitative assessment of the errors involved in current predictions due to scaling assumptions, using an EBM to explore the model response to forcing scenarios used in current predictions (Nakicenovic et al. (2000)). Again the use of EBM models allows us the flexibility to address this question for the whole range of model parameters in a vastly less computationally expensive manner than a similar approach using large multi-model ensembles (such as suggested by www.climateprediction.com).

Energy Balance Models (EBMs) are able to reproduce many of the features of the global temperature response of the full Atmosphere-Ocean coupled Global Circulation Models (AOGCMs). The temperature response of an individual EBM can be tailored to the AOGCM response by careful selection of model parameters. It is this property of EBMs which has seen extensive use made of them to extend the range of future scenarios for which temperature forecasts are made (Raper and Cabasch (1996), Raper et al. (2001) and Cubasch et al. (2001) to name but a few). Figure 4 shows the temperature response of HadCM3 to the A1FI (see below) scenario (dashed line) and 20 EBM simulations which closely fit the AOGCM's response. These EBM runs each contain different parameterisations of the climate sensitivity and ocean diffusivity yet each is able to reproduce the more complex models response. If we had chosen to fit the EBM to a HadCM3 runs driven by a scenarios with stabilisation behaviour, we would expect the number of runs which are consistent with the result to be much more tightly constrained (as the differences in stabilisation behaviour become more apparent). The fact that a number of EBM simulations are able to reproduce the HadCM3 response for the A1FI scenario is illustrative of the scaling assumption that current climate forecasts rely on.

Climate predictions quoted in the latest IPCC report (Cubasch et al. (2001)) suggest temperature rises between 1.4 - 5.8 by 2100. This is based on an inter-model spread of future predictions and as such does not attempt to assess the likelihood of a given forecast model reproducing the real climate response. Stott and Kettleborough (2001) produced a probabilistic estimate based on uncertainties in radiative forcing of the temperature response in 2100 of 1.4 - 7 K (for the A1FI SRES emission scenario, Ramaswamy et al. (2001)). Current uncertainty analysis for these predictions makes no quantitative statement of the additional error associated with possible breakdown in the scaling relationship between models other

than noting that there is potential for errors to wards the end of the predictive period. The future projected scenarios of anthropogenic emissions are based on a range of projected changes in energy consumption due to changes in technology use or economic development and are known as the SRES scenarios (Ramaswamy et al. (2001)). Errors in scale-ability of the model are dependent on the forcing profile. Differences between the SRES scenarios can be expected to produce different uncertainty bounds due to parameter uncertainty of the key climate variables.

Figure 1.3 shows the total anthropogenic radiative forcing for four SRES scenarios, A1FI, A2, B1 and B2 along with their corresponding green house gas (ghg) forcing and other forcing components (which combine to form the total forcing). We can see from figure 1.3 that all four total forcing components of the SRES scenarios are fairly close to a s steadily increasing forcing profile. A1FI shows the total forcing rate continuing to accelerate from 2000 to 2050. The other 3 scenarios show a steadier increase in the forcing over the same period with some indication of a slowing down in the rate of increase, with perhaps the B1 scenario responding most in this way. On the basis of the earlier work with the simple representations and the idealised step change experiments we can expect the errors to be greatest in magnitude for the B1 scenario while the A1FI scenario would remain fairly error free - at least for the first 50 years of prediction. An assessment can also be made of the scaling assumption error for the individual components of the total forcing (green house gas component (purple) and the other forcing components (green)). The green house gas (ghg) component shows a similar behaviour to the total forcing but shows a greater degree of stabilisation in the later 21st century (and so would be expected to show larger magnitude of errors). The aerosol forcing component is perhaps the most interesting showing complete stabilisation by 2050 in all scenarios apart from A2 which stabilises shortly after. Errors associated with these components are likely to be much larger in their magnitude (the magnitude of the aerosol component is small overall, compared to the ghg component and as such the impact of this uncertainty is likely to be correspondingly smaller). The degree to which uncertainties, due to scaling assumptions, cancel for the two components (ghg and aerosol) is not known. As such, uncertainty assessments on future predictions need to take account of the errors of the individual components rather than the errors associated with the total forcing.

1.4.1 Exploring scalability of predictions

To explore the impact of scaling assumptions on uncertainty in future forecasts, the EBM model was setup to simulate the temperature response in the parameter space for the total Forcing, green house gas component and the Other Forcing component of each of the four SRES scenarios (a total of 12 forcing

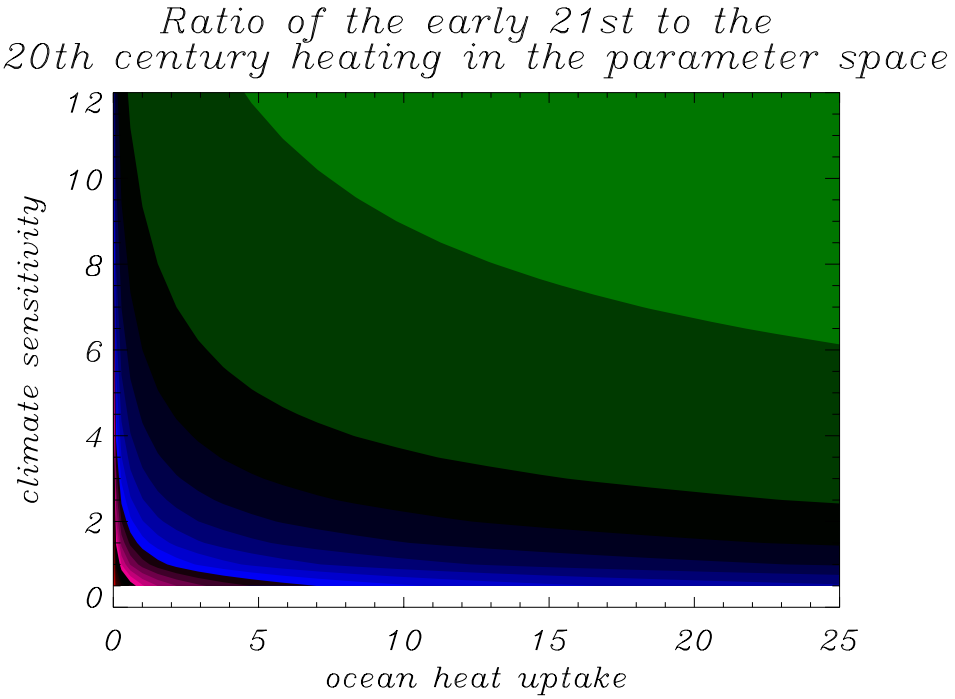

Figure 1.2: . The plot shows the ratio of early 21th century warming to the 20th century warming for a range of 900 parameters in the parameter space in response to a step change in forcing in 1800. The timescale is nominally chosen so show the scale-ability of the response in a later period (between 100-150 years) to the an earlier warming period (100 year). This typically is the timescale of interest when comparing the predicted warming using a GCM with the representation of past temperature. The plot illustrates the scale-ability of the response through the parameter range. Parameter points which lie on the same contours on the plot share the same scaling relationship between the latter warming period and the early warming period. The number of contours increase as either climate sensitivity or ocean diffusivity decrease with the contours most tightly packed around the small sensitivity and small ocean diffusivity region. This reflects stabilisation of the temperature realisations for the regions of parameter space with shorter timescales of response (small climate sensitivity and small K_v). The greater the number of contours between parameter combinations the greater breakdown in the scale-ability of responses.

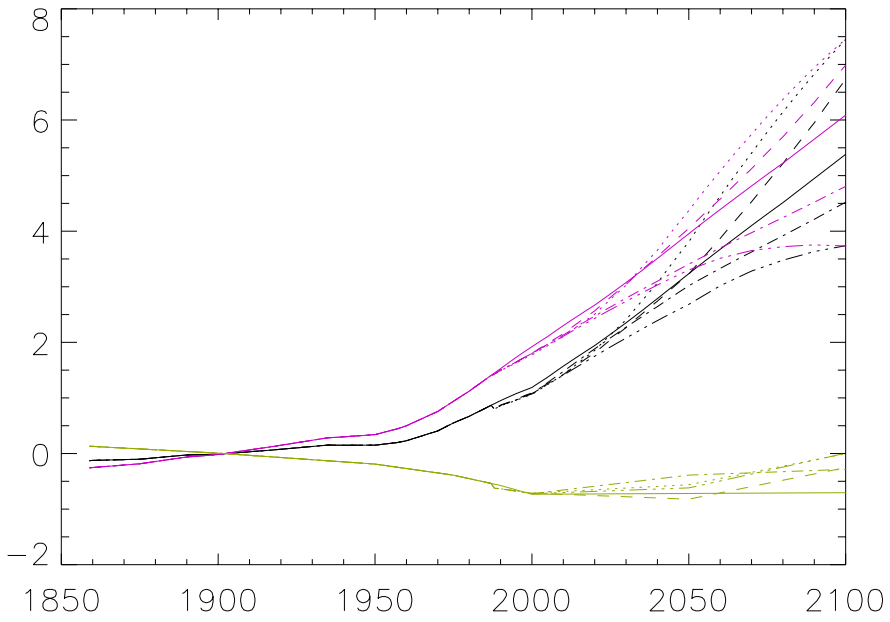

Figure 1.3: .The plot shows the climate forcing scenarios for 4 SRES scenarios and the IS92a scenario with their Green House Gas and the Aerosol Components in Watts/ m2. The strong black lines represent the Total anthropogenic forcing for the four SRES scenarios, A1FI (dot-dot); A2 (long dash); B1 (dot-dot-dot-dash) and the B2 (dot-dash) scenarios, along with the IS92a scenario (solid line). The total anthropogenic component has been separated into the Green House Gas component and the Aerosol only component. The purple lines represent the Greenhouse Gas Component of the forcing profiles. The Green lines show the Other Forcing components of the SRES scenarios and the Aerosol Only component of the IS92a scenario (represented by the appropriate lines). The SRES scenarios represent future 'narrative' story lines for future changes in technology use and economic development. Emissions of the principle green house gases as well as other anthropogenic emissions are estimated for each scenario. Models have then been used to calculated the resulting radiative flux at the top of the atmosphere as a result of this change. The four of these scenarios have been chosen which represents the range of behaviour in the complete set of SRES scenarios.

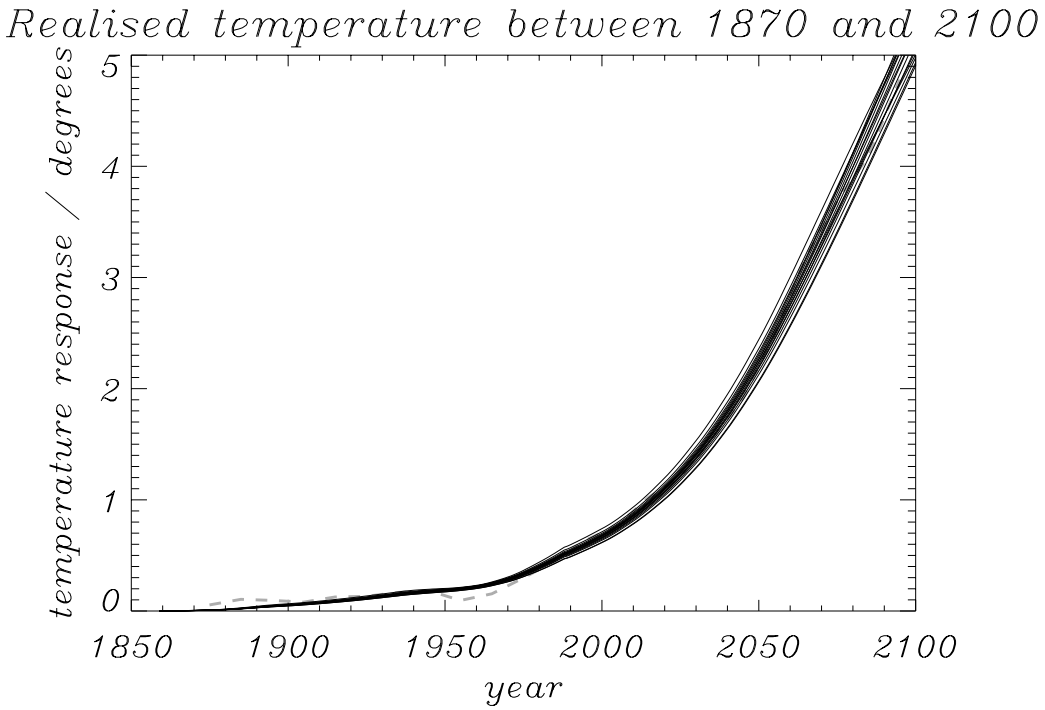

Figure 1.4: . The plot shows the temperature realisation of HadCM3 (dashed green) in response to historical forcing by anthropogenic changes and by future forcing using atmosphere compositional changes predicted in the A1F1 SRES scenario. The black lines show 20 temperature realisations using the energy balance model representing 20 different parameter combinations of climate sensitivity and ocean diffusivity. The energy balance model is able to reproduce much of the predicted temperature response of the GCM. Differences are evident in the early simulation (1860 - 2000). The EBM runs for this period are forced by radiative fluxes at the top of the atmosphere (calculated using HadCM2). The differences between the temperature response between HadCM3 and the EBM in the early integration can be partly attributed to the model differences between HadCM3 and the radiative forcing calculated with HadCM2. Better match is observed from 2000 from which point the EBM uses radiative forcing calculated from HadCM3.

profiles). The net affect of the Other Forcing component on the surface temperature is a negative one which counteracts the warming affect of the greenhouse forcing. Their combined temperature response accounts for the total anthropogenic surface temperature response, however errors associated with these individual components of the forcing can not necessarily be assumed to cancel in the consideration of the total error associated with each scenario. In the context of a systematic study of uncertainties in climate prediction, it is important to assess these components individually. For each forcing profile, 900 simulations of the Energy Balance Model's surface temperature response are carried out (representing a regular grid in parameter space with values of the Climate Sensitivity between 0.5 and 15 K and values of Ocean Diffusivity between 0.03 and 50 cm^2s^{-1}).

To test the additional uncertainty introduced into future predictions due to the the break down in the scaling assumption, the difference between the model response and a predicted response based on a reference scaling relationship is calculated for each parameter combination. The reference scaling relationship is calculated from the 1900-2000 temperature response and the future temperature response in the EBM, using parameter values consistent with the AOGCM, HadCM2 (Climate Sensitivity of 2.5 K and Ocean Diffusivity of 8 cm^2s^{-1}). This is used make a predictive temperature response for each of the model parameterisations, by scaling the 1900-2000 temperature response for each combination by this reference scaling relationship. The assessment of the error involved in scale-ability is calculated for 2050 (for comparison with the Allen et al. (2000)) and for 2100 (for comparison with Stott and Kettleborough (2001)).

As discussed earlier, errors in the scale-ability of the response are expected to be observed for forcing profiles which begin to show stabilising behaviour. Figures 5 and 6 show the error in 2050 associated with the parameter space for the Total Forcing component of A1FI and B1 SRES scenarios respectively. The plots are made for a parameter space up to values of climate sensitivity of 12 K and Ocean Diffusivity of 25 cm^2s^{-1}. The magnitude of the error for all four SRES scenarios remains consistently small for the whole parameter space, with the response being most consistent with the scale-ability assumption in the A1FI scenario (predictive errors don't exceed 2% of the realised temperature). The B1 error response is plotted (figure 6) as the SRES scenario with the largest error in 2050. As noted of figure 4 earlier, the B1 scenario shows the greatest tendency to wards a slow down in the increase in forcing at 2050. The errors evident in the low sensitivity, low ocean diffusivity region are indicative of the stabilisation pattern predicted in the stabilisation study (fig. 2). The models, in this region with the shorter response time scales, are responding to the slow down in the increase in forcing in this scenario, while the scale-ability of response in the majority of the parameter space is still indistinguishable for the models with longer response time scales. The error in the B1 scenario is not particularly large, exceeding -10% of

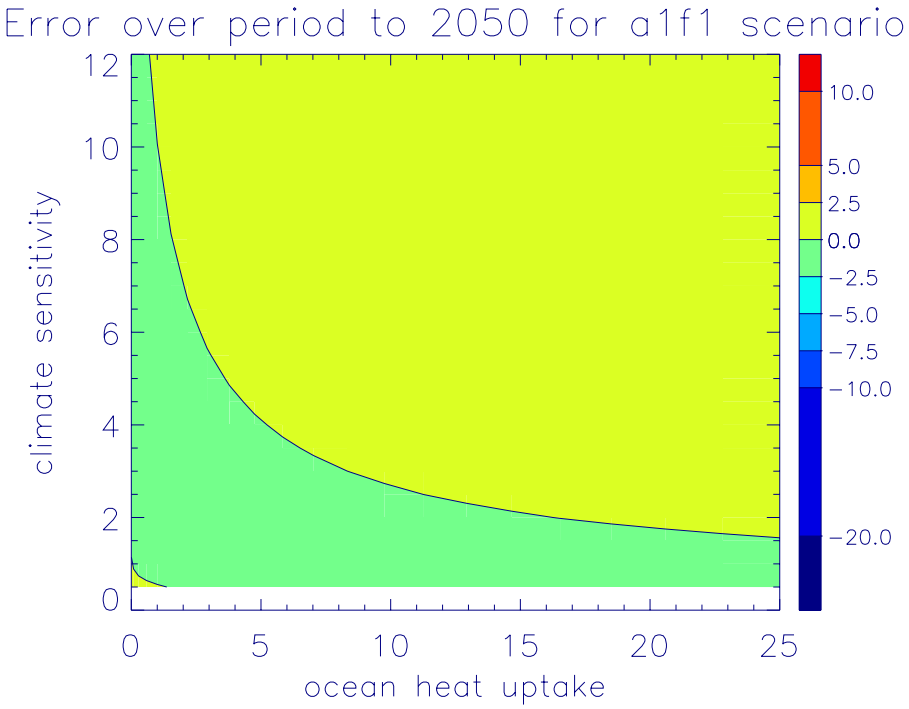

Figure 1.5: . The plot shows the percentage error due to assuming that the model temperature response in 2050 will scale to the model response corresponding to parameter combinations used by HadCM2 for the A1F1 forcing scenario. The error for the entire parameter space remains small for this scenario in 2050. Errors in the scale-ability of the temperature response would be expected in regions of the parameter space which respond on short enough timescales for differences in stabilisation to occur. The response of the model to step changes in forcing indicates that the low sensitivity and low ocean diffusivity region of parameter space is where errors are likely to be evident. The steady increase of the forcing up till 2050 means that stabilisation behaviour is not able to occur at this stage in the A1F1 scenario and errors due to the scaling assumption are therefore limited to +-2.5%.

the predicted temperature response in 2050. The error in this region of parameter space is difficult to rule out as inconsistent with the current climate. Recent attribution studies (Forest et al. (2000), Forest et al. (2002)) attempt to place constraints on the range of climate sensitivities and ocean diffusivities consistent with the observed record, succeeding in limiting the upper and very low climate sensitivity range. However in this study, the region containing the larger errors lies within the parameter space, consistent with past changes. The spatial pattern of the error associated with the scaling relationship in the B1 SRES scenario in 2050 is illustrative of the general pattern of response in all scenarios producing errors in this study, with only the magnitude and size of the region increasing with the increase of the magnitude of the error.

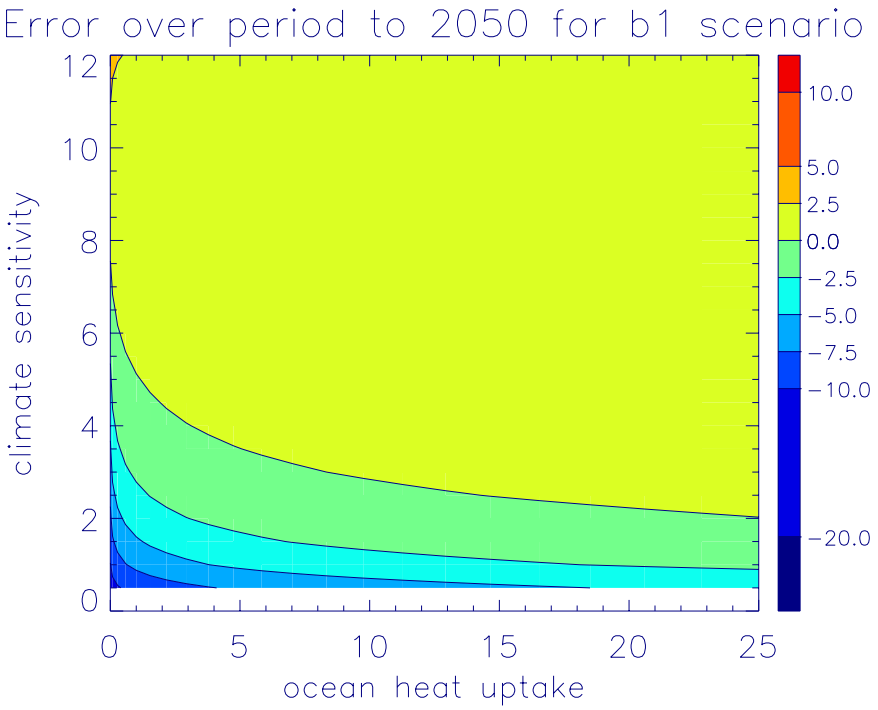

Figure 1.6: . The plot shows the percentage error due to predicting the model temperature response in 2050 with the relationship between past and future temperature using the parameter combinations found in HadCM2, for the B1 forcing scenario. Contrasting to the error in scaling assumption in the A1F1 forcing scenario, the break down in scale-ability is more evident in the B1 scenario in 2050. Of the 4 SRES scenarios B1 shows the greatest tendency towards a stabilisation of forcing although by 2050 the differences in total forcing between the 4 scenarios are still fairly small. The differences are sufficient however to result in increased error in the small sensitivity, small ocean diffusivity region as model parameter combinations in this regions start to show stabilisation behaviour. The errors themselves remain small, with realised temperatures exceeding -10% of the predicted temperature in only one model parameter combination. The bulk of the parameter space contains error with less then +-2.5%. The region of higher error can't be discounted however as being incompatible with the real climate. The stabilisation in the forcing scenario is not sufficient to cause significant breakdown in the scale-ability relationship.

Histograms of the errors associated with the scaling assumption for the four SRES scenarios in 2050 and 2100 are illustrated in figures 7 and 8 respectively. It is apparent that the errors for most of the parameter space are small with only a small tail of parameter combinations contributing a larger error in the response. In 2050 the 10% to 90% distribution bounds lie within a region between +/-2.5% error. By the end of the century, errors due to using a scalability assumption have grown. The region of parameter space with the shorter response times shows errors in excess of -30% for all 4 scenarios (including A1FI). The magnitude for this error in the B1 scenario is the largest as expected, exceeding -45% of the temperature response predicted by the scaling relationship. Again, although this error is only found in a small portion of the parameter space it is currently not possible to rule out this region as being inconsistent with the parameters in the real climate, Forest et al. (2000). Again, most of the parameter space produces only small errors due to the break down in the scale-ability relationship (the 10% to 90% distribution all lie between the +/-10% for all scenarios). The 4 SRES scenarios show good agreement in their errors. There is a positive bias to the error however, with median values all exceeding +5% error. This can be accounted for by the shorter response time scale of the reference scaling relationship (chosen in this analysis to match HadCM2) which would tend to predict smaller temperature responses in the parameter space with longer response times.

Considering the errors in response to the individual components of the anthropogenic forcing profile (the green house gas only component and the other forcing component) identical analysis of the respective forcing profiles is carried out. The errors in the temperature response to the green house gas forcing component are similar to the errors in the response of the total anthropogenic forcing component with the B1 and B2 scenarios showing marginally larger errors in 2050. The errors are larger than the errors associated with the total forcing component in 2100 for all the scenarios. The Other forcing component is more interesting however. Throughout the 20th century there was a steady increase in the strength of the forcing, mainly due to the increase in aerosol loading. During 2000-2050 the SRES scenarios predict a reduction in the rate of the forcing.

Figures 9 and 10 show the histograms and error distributions for the model driven by the Other forcing component for the four SRES scenarios in 2050 and 2100 respectfully. The much larger negative tail to the error in all scenarios is immediately obvious. By 2050 errors associated with making a scaling assumption in the predictions, reach as high as 68% in the B1 scenario. The A2 Other forcing component is the least prone to errors in this assumption with the bulk of the parameter space (between 10% and 90% distribution bounds) constrained to a 13% error range centred over zero (compared to a 23% range for the B2 scenario). By 2050 the Other forcing component of the A2 SRES scenario is the only component not to have reached complete stabilisation. As for the distribution of error in the 2100 response to the

Error associated with the Total Forcing component of the scenarios, in 2050

(a) Histogram

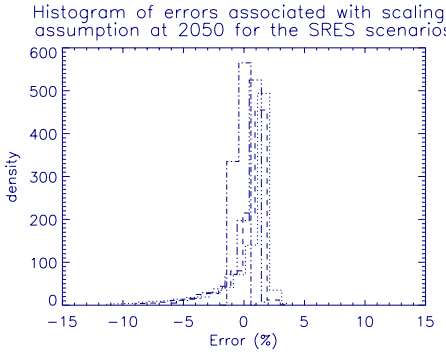

(b) Distribution

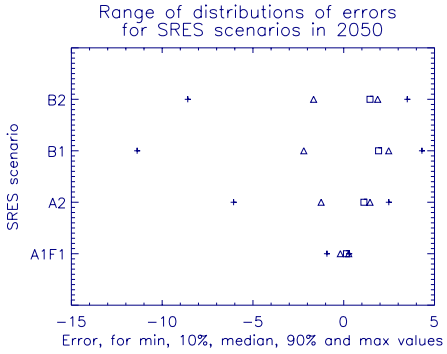

Figure 1.7: . The histogram (a) shows the error associated with the scaling assumption for the 4 SRES scenarios, A1F1 (dot-dash); A2 (dot-dot-dot-dash); B1 (dot-dot) and B2 (long dash) in 2050. The errors in 2050 are minimal with the majority of the parameter space exhibiting errors between +-2.5%. With the exception of the A1F1 scenario, the model produced a tail of larger errors for the scenarios, with the B1 scenario exceeding errors of -11%. This tail contains only a small number of parameter combinations but these remain difficult to discount as being incompatible with the real climate. The distribution of errors (b) show the range of errors associated with each scenario in 2050 for the total forcing. The plot shows the greatest negative and positive values of the error (crosses), the 10% and 90% error bounds (triangles) for the PDF of the error and the median value (square) for each of the scenarios. The differences between the negative error in is evident between the scenarios but the distribution of error between the 10 and 90% range remains remarkable similar for the A2, B1, and B2 scenarios with the A1F1 distribution even more tightly constrained.

Error associated with the Total Forcing component of the scenarios, in 2100

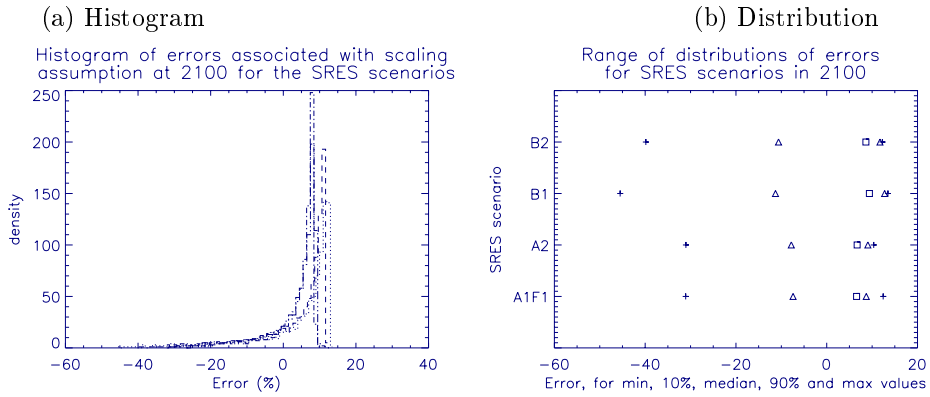

Figure 1.8: . The histogram (a) shows the error associated with the scaling assumption for the 4 SRES scenarios, A1F1 (dot-dash); A2 (dot-dot-dot-dash); B1 (dot-dot) and B2 (long dash) for the total forcing in 2100. Contrasting with the errors in the scale-ability of the response in 2050, the magnitude of the negative error tail is much larger in 2100. The forcing profiles for all scenarios exhibit some degree of slow down (fig. 3) by the end of the 21st century and this is evident in the magnitude of the negative error in the tail of the histogram as the parameter combinations with the smallest timescales of response react to the stabilisation. The bulk of the error for this region is lies between +-10% with a strong weighting towards positive errors between +5-10%. The parameter combination chosen for the scaling relationship corresponds to the value derived from HadCM2. This parameter combination in the model has a timescale of response which results in stabilisation towards a smaller temperature then predicted by the scaling properties of the bulk of the parameter space (whose stabilisation response wont become apparent until later) by 2100. The longer response timescales of the parameter space (and corresponding lack of stabilisation) accounts for the positive bias of the errors in the histogram. The distribution (b) of errors show the range of errors in 2100 associated with each scenario. The plot shows the greatest negative and positive values of the error (crosses), the 10% and 90% error bounds (triangles) for the PDF of the error and the median value (square) for each of the scenarios. The differences in the magnitude of the negative error for the four scenarios again are evident with the largest error apparent in the B1 scenario. The 10% to 90% bounds are remarkable similar for all 4 scenarios, with the positive bias again evident by the median value.

Error associated with the Other Forcing component of the scenarios, in 2050

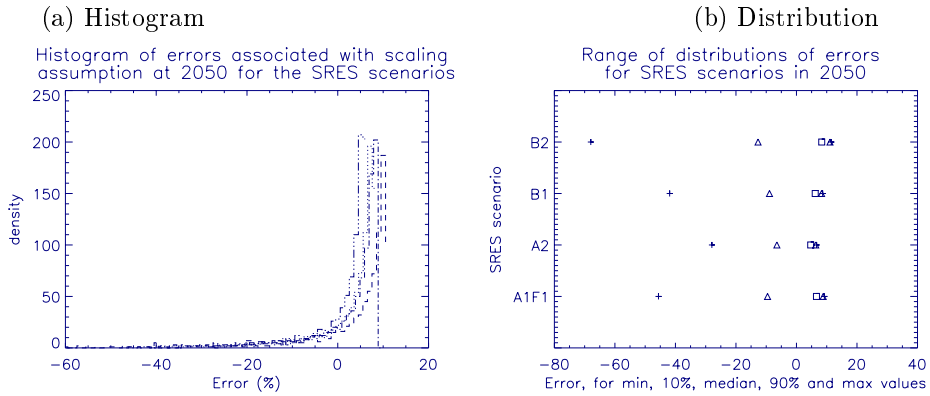

Figure 1.9: . The histogram (a) shows the error associated with the scaling assumption for the 4 SRES scenarios, A1F1 (dot-dash); A2 (dot-dot-dot-dash); B1 (dot-dot) and B2 (long dash) in 2050. All 4 scenarios contain large negative error tails (exceeding -70% in the case of the B1 Scenario). The error associated with these parameter combinations, although constituting a small fraction of the total distribution of errors, is difficult to rule out as inconsisitant with the real climate. The bulk of the error density falls within a 20% error band, with a bias towards a positive error with respect to the reference scaling parameter combination. The distribution of errors (b) show the range of errors associated with each scenario in 2050 for the Other forcing components. The plot shows the greatest negative and positive values of the error (crosses), the 10% and 90% error bounds (triangles) for the PDF of the error and the median value (square) for each of the scenarios. The difference in the magnitude of the negative error between the models is evident. In response to the Other Forcing component the B2 scenario response shows the greatest error, while the A2 response is much smaller. Again the differences between the bulk of the error distributions for the 4 scenarios is less significant compared to the differences in absolute error, with the A2 distribution most constrained (error range of 13% between the 10% and 90% distribution bounds) and the B2 scenario with the widest range (with and error range of 23% between the 10 and 90% distribution bounds).

total forcing components there is a marked positive bias to the median values of the error.

The tendency for larger errors for the later time in the model prediction is also evident in the response to the other forcing component (figure 1.10). The picture for all 4 scenarios is more consistent with peak errors approaching -80% in all scenarios. The errors in each forcing scenario, follow a similar pattern to the errors in figure 1.6 with only the magnitude and the area covered by by the errors increasing with the size of the maximum error. The region of parameter space with low sensitivity and low ocean heat uptake shows the greatest sensitivity to errors in the scale-ability. This is due to the more rapid response time scales in this region which are able to respond to reductions and stabilisations in the forcing more rapidly than the bulk of the parameter space.

The error distribution for the bulk of the parameter space is larger in 2100 with 80% of model runs showing errors between +/-20%, figure 1.10. The positive bias to the error distribution is more evident with the majority of the parameter space showing errors in excess of +18% of the predicted temperature

Error associated with the Other Forcing component of the scenarios, in 2100

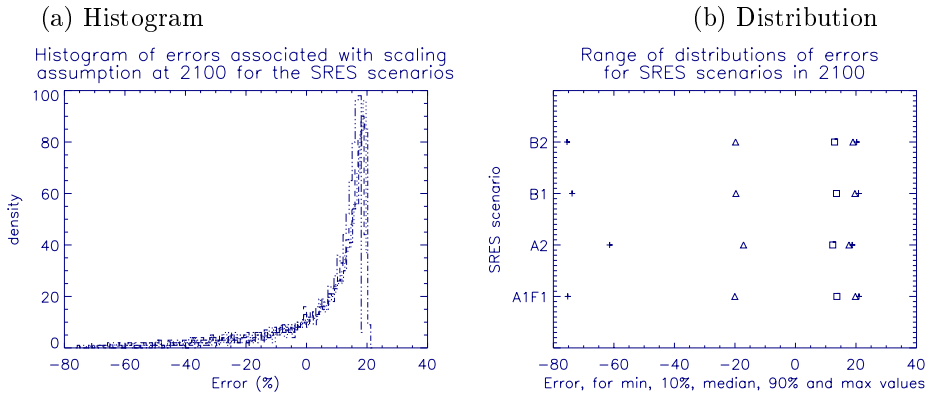

Figure 1.10: . The histogram (a) shows the error associated with the scaling assumption for the 4 SRES scenarios, A1F1 (dot-dash); A2 (dot-dot-dot-dash); B1 (dot-dot) and B2 (long dash) in 2100. All 4 Scenarios show larger errors for the Other forcing components, than in 2050. The distribution of errors (b) shows the errors associated with the Other components of the forcing are remarkably similar for all the scenarios. The distribution of the errors associated with the bulk of parameter space covers a much larger area than the earlier errors (with 80% of the parameter spacewith errors ranging between +-20% with a strong bias towards a positive error (median error values averaging +19.0% for the scenarios)

response (the median values average at +19% for all the scenarios). The magnitude of this error and the size of the parameter space which exhibits this error causes concern over for the assessment of the total uncertainty of predictions in 2100. The effect of this error on the assessment of uncertainties is tempered however by the much smaller impact that the Other forcing scenarios has on the total temperature response to anthropogenic forcing compared to the green house gas component. Future ghg forcing scenarios, which might result from emission trends following the potential for a concerted policy intervention to stabilise CO_2 levels, could be expected to show a similar pattern.

1.5 Discussion

We have shown that uncertainties in two key climate parameters (climate sensitivity and heat uptake by the deeper ocean) makes constraining long term climate predictions problematic. However, at shorter time scales (decadal to century), the assumption that future climate changes will scale similarly to the past changes (across the range of parameter uncertainty) is fundamental to the current assessment of uncertainty in climate forecasts. The degree to which uncertainties in the key parameters contribute to forecast uncertainty is dependent on the nature of the forcing. We have used a simple energy balance model (EBM) to explore the global temperature responses for an idealised stabilisation case, to illustrate

the scope for errors to be introduced due to the break down in scale-ability across the range of accepted parameterisations. We have further extended the analysis to consider the EBM response to the radiative forcing resulting from four SRES anthropogenic emission scenarios. The forcing profiles increase fairly steadily throughout the time period with only marginal stabilisation behaviour to wards 2100. As expected, errors due to the break down in scale-ability are minimal for the bulk of the parameterisations for all 4 scenarios. However by the end of the century small regions of parameter space (low sensitivity and low ocean diffusivity) show significant errors in the scaling assumption. While these regions remain a minority of the parameter space of interest, they currently can not be excluded on the basis of being inconsistent with past climate. Errors are sufficiently large to warrant inclusion in uncertainty analysis of future forecasts using these scenarios.

Consideration of future uncertainty is further complicated by consideration of error involved in individual components of the future emissions scenarios. It is not clear whether the errors involved in individual components of the SRES scenarios cancel in the reproductions of the total forcing. As such it is perhaps necessary to consider the error associated with the components of the forcing in future uncertainty assessments. The aerosol (other forcings) component in particular shows large errors due to break down in the scaling relationship as the forcing profile stabilises. The relatively small impact of this component compared to the Green House Gas component needs to be taken into account, however any treatment of uncertainty (due to scaling assumptions) which addresses the individual components, is likely to show larger error bounds to an approach which deals with just the total forcing.

The magnitude of the errors produced in this study are relative to the temperature response of the reference scaling relationship, which in this case is based on HadCM2. The shape of the histogram for any of the scenarios analysed is independent of which model is chosen for the reference scaling relationship. However the magnitude of the errors is not, as the errors for each point on the parameter space are relative to the reference scaling parameterisation (chosen in most cases to be the parameterisation of the AOGCM on which the uncertainty analysis is being carried out). If the reference scaling relationship used was selected to reproduce the NCAR AOGCM for instance, which has very low heat penetration into the deeper ocean, then the resulting histogram would show mainly positive errors with the majority of the points in the large and positive region of each histogram.

The follow-up paper (Forest et al. (2002)) to Forest et al. (2000) further constrains the parameter region consistent with the observed climate record by incorporating recent data on ocean heat uptake (Levitus et al. (2000)). This enables an upper limit to be placed on climate sensitivity for the first time. The analysis produced in this chapter could be repeated to account for the upper limit. This is likely to

reduce the upper error limit on the histograms marginally (as the large sensitivity parameterisations tend to have the longer response times), but is unlikely to restrict the larger errors in the negative tail of the histograms. This is because the region of parameter space which is most sensitive to errors in the scaling relationship lies in the region of low sensitivity and low ocean heat uptake. Forest et al. (2002) is unable to make further constraints on the lower sensitivity bound (at 0.5 K) and low deep ocean heat uptake from their earlier paper.

Assessment of the impact of uncertainty in climate sensitivity and penetration of heat to the deeper ocean is even more important to address for forecasts based on potential future emission scenarios resulting from concerted inter-governmental intervention to stabilise CO2 levels. While the likelihood of this remains firmly in the political arena, uncertainty in stabilisation scenarios remains difficult to address with individual AOGCMs, and requires an approach similar to the one taken in this chapter or a similar approach to that being taken by www.climateprediction.com. Scenarios with stabilisation of emissions of green house gases is likely to introduce further uncertainties in forecasts as stabilisation responses start to be observed in some of the parameter space. Although century scale forecasts for 'business as usual' emission scenarios are likely to be less dependent on parameterisation of the key climate parameters the usefulness of the EBM as a tool to make such assessments diminishes as projected temperatures rise. The EBM is inherently a linear model. As the size of the warming becomes larger it becomes increasingly difficult to rule out significant non-linear feedbacks. Large temperature projections require the use of models which are able to capture these feedback processes and as such a more thorough approach would need to be made using multi-member, multi-model AOGCM ensembles (climateprediction.com). However the EBM remains a useful tool to rapidly assess likely error bounds for current emission scenarios, as well as place more confident probability density functions for the more modest stabilisations.

Bibliography

Myles R. Allen, Peter A. Stott, John F. B. Mitchell, Reiner Schnur, and Thomas L. Delworth. Quantifying the uncertainty in forcasts of anthropogenic climate change. *Nature*, 407:617–620, 2000.

U. Cubasch, G. A. Meechl, G. J. Boer, R. J. Stouffer, M. Dix, A. Noda, C. A. Senior, S. Raper, and K. S Yap. Projections of future climate change. *chapter 9, IPCC, Working Group 1*, 2001.

Chris E. Forest, Myles R. Allen, Peter H. Stone, and Andrei P. Sokolov. Constraining uncertainties in climate models using climate change detection techneques. *GRL*, 27:569–572, 2000.

Chris E. Forest, Peter H. Stone, Andrei P. Sokolov, Myles R. Allen, and Mort D. Webster. Quantifying uncertainties in climate system properties with the use of recent climate observations. *Science*, 295: 113–117, 2002.

J. Hansen, A. Lacis, D. Rind, and G. Russell. Climate sensitivity: analysis of feedback mechanisms. 1980.

J. P. Holman. *Heat Transfer*. McGraw-Hill Book Company, 1986.

A. Kattenberg, F. Giorgi, H. Grassl, G. A. Meechl, J. F. B. Mitchell, R. J. Stouffer, T. Tokioka, A. J. Weaver, and T. M. L. Wigley. Climate models - projections of future climate. *IPCC, Working Group I report*, pages 363–443, 1996.

Sydney Levitus, John I. Antonov, Timothy P. Boyer, and Cathy Stephens. Warming of the world ocean. *Science*, 287:2225–2229, 2000.

N. Nakicenovic, J. Alcamo, G. Davies, B. de Vries, J. Fenhann, S. Gaffin, K. Gregory, A. Grubler, T. Y. Jung, T. Kram, E. L. La Rovere, L. Michaelis, S. Mori, T. Morita, W. Pepper, H. Pitcher, L. Price, K. Raihi, A. Roehrl, H-H. Rogner, A. Sankovski, M. Schlesinger, P. Shukla, S. Smith, R. Swart adn S. Van Rooijen, N. Victor, and Z. Dadi. *IPCC special report on Emissions Scenarios*. Cambridge University Press, 2000.

V. Ramaswamy, O. Boucher, J. Haigh, D. Hauglustaine, J. Haywood, G. Myhre, T. Nakajima, G. Y. Shi, and S Solomon. Radiative forcing of climate change - chapter 6 IPCC third assessment report, 2001.

S. C. B. Raper and U. Cabasch. Emulation of the results of a coupled general circulation model using a simple climate model. *GRL*, 23:1107–1110, 1996.

S. C. B. Raper, J. M. Gregory, and T. J. Osborn. Use of an upwelling-diffusion energy balance climate model to simulate and diagnose A/OGCM results. *Climate Dynamics*, 17:601–613, 2001.

C. A. Senior and John F. B. Mitchell. The time dependance of climate sensitivity. *Hadley Centre Report*, 2000.

A. P. Sokolov and P. H. Stone. Global warming projections: Sensitivity to deep ocean mixing. *MIT Report*, 1996.

A. P. Sokolov and P. H. Stone. A flexible cliamte model for use in integrated assessments. *Climate Dynamics*, 14:291–303, 1998.

P. A. Stott and J. A. Kettleborough. The impact of uncertaintiy in anthropogenic emissions on predictions of twenty first century climate change. *Submitted to nature*, 2001.